Technical Note

Modifications to the Single Point Velocity Measurement Method for Estimating River Discharge in Low-Resource Environments

Ghadeer Ali[1] and Mahmoud F. Maghrebi[2]

Abstract: Accurate and reliable river discharge evaluation at a river station is an essential piece of information to obtain. This work modifies a power-law (PL)-based model and a single point velocity measurement (SPM) method for calculating channel discharge. Specifically, modifications are proposed for the constant shear velocity assumption, water surface effects, the underlying velocity distribution, and the number of measurements. A coefficient of water surface (cw) is proposed to consider the impact of water surface on distribution of velocity. Additionally, a power-wake-law (PWL) method is proposed to cope with the velocity dip phenomenon, where the maximum velocity occurs below the water surface. A critical assessment of the performance of the modifications using laboratory and field data is introduced. A trial-and-error procedure is applied to the laboratory data to obtain the value of the proposed coefficient cw and the parameters of PWL velocity distribution, α and β. It is found that $cw = 0.3$, $\alpha = 1.5/\text{m}$, and $\beta = 0.6$ are the most appropriate values that produce minimum errors in most cases. A combination approach is applied to the field data to demonstrate the performance of the modifications and the impact of increasing the number of measurements. It is found that considering a water surface effect has significantly improved the accuracy. Also, it is found that the modified PL- and PWL-based models can estimate discharge with a reasonable accuracy using five measured velocimetry points in most tested cross-sections. In most studied rivers, the five-point combinations reduce the mean absolute percentage error (MAPE) value to less than 5%. **DOI: 10.1061/JHEND8.HYENG-13469.**

Author keywords: Velocity profile; Discharge estimation; Dip phenomenon; Yellow River; Edo River; Power law.

Introduction

Efficient algorithms for extracting mean cross-sectional channel velocity from local measures of velocity within a cross-section are useful for estimating river discharge. Primarily, approaches that evaluate the mean channel velocity from water surface velocity are based on the velocity index method or the probability concept (e.g., Welber et al. 2016; Fulton et al. 2020). Other discharge estimation methods utilize the observed water velocity from a limited portion of the cross-section. Maghrebi (2006), based on computed velocity contours and only one observed point velocity, proposed the power-law (PL)-based model and the single point velocity measurement (SPM) method for calculating discharge in channels. Although the results of this method demonstrate a good agreement with measured data, there are still some areas for improvement in fitting vertical velocity profiles and hence in estimating the discharge. The main objective of this work is to introduce modifications to the PL-based model to enhance its accuracy. Modifications are proposed with regard to the constant shear velocity assumption, water surface effects, the underlying velocity distribution, and the number of measurements.

The current study has been conducted with the following specific objectives:

1. To obtain the appropriate value of water surface coefficient cw.
2. To explore the use of the power-wake-law (PWL) velocity distribution as a velocity function and obtain its parameters, α and β.
3. To consider using multipoint measurements with the arithmetic average instead of single-point measurement.
4. To provide recommendations on the preference of the location of a single measurement point.

Methods and Data

Cross-Sectional Isovel Contours

Maghrebi (2006) introduced a mathematical model to evaluate the velocity distribution in an arbitrary cross-section. In this method, as shown in Fig. 1, the channel cross-section is covered with a triangular mesh, and the boundary is divided into infinitesimal elements $d\mathbf{s}$. The velocity deviation at the center of the mesh element can be calculated as follows:

$$\mathrm{u} = \int_{boundary} c_1 \sin(\theta) f(r) d\mathbf{s} \tag{1}$$

where c_1 is a constant, θ is the angle between the positional vector $\mathbf{r}$ and the boundary elemental vector $d\mathbf{s}$, and $f(r)$ is the velocity function. Maghrebi and Ball (2006) used the seventh root power law as a velocity function. Therefore, the local velocity $u(y, z)$ at each element can be computed as

[1]Ph.D. Candidate, Dept. of Civil Engineering, Ferdowsi Univ. of Mashhad, Mashhad 91775-1111, Iran. ORCID: https://orcid.org/0000-0002-1631-7374

[2]Professor, Dept. of Civil Engineering, Ferdowsi Univ. of Mashhad, Mashhad 91775-1111, Iran (corresponding author). ORCID: https://orcid.org/0000-0002-0082-0020. Email: maghrebi@um.ac.ir

Note. This manuscript was submitted on August 24, 2022; approved on June 19, 2023; published online on September 7, 2023. Discussion period open until February 7, 2024; separate discussions must be submitted for individual papers. This technical note is part of the ***Journal of Hydraulic Engineering***, © ASCE, ISSN 0733-9429.

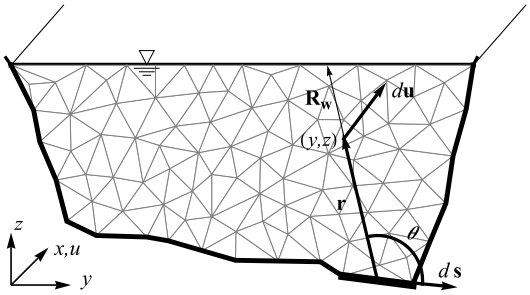

Fig. 1. Impact of boundary elements on an arbitrary point in a river section.

$$u(y,z) = \int_{boundary} cu_* \sin\theta r^{1/m} d\mathbf{s} \tag{2}$$

where c is a coefficient related to the boundary geometry and relative roughness, u_* is the shear velocity, and $m = 7$. The shear stress distribution along the boundaries in regular channels, except for the area close to corners, is uniform. Therefore, Maghrebi (2006) took u_* as a constant. Normalizing the local velocity using the mean velocity U and writing it in finite difference form yields

$$C(y,z) = \frac{u(y,z)}{U} = \frac{\sum_{boundary} c \sin\theta r^{1/m} d\mathbf{s}}{\frac{1}{A}\sum_A \left(\sum_{boundary} c \sin\theta r^{1/m} d\mathbf{s}\right) dA} \tag{3}$$

where $C(y,z)$ is the normalized local velocity and A is the cross-sectional area.

Boundary Effects

The coefficient c in Eq. (2) represents a resistance that determines the effect of the wall on the whole cross-section. It mainly depends on the roughness and shape. The coefficient c takes smaller values for rougher boundaries and equals unity and zero for uniform boundary roughness and free water surface, respectively. Maghrebi (2006) examined the model in rectangular experimental channels. Although the computed velocity profile showed a good agreement with the data, the model overestimates the velocity near the water surface and underestimates it near the bed.

The first step of this work is to overcome the aforementioned issue. Therefore, it is suggested that the coefficient c for the water surface cw is not equal to zero anymore and should be obtained. The analysis of cw effect is introduced in the "Results" section.

Boundary Shear Stress

For uniform flow conditions in wide channels, the boundary shear stress, and hence the shear velocity, is widely computed through a force balance approach given by

$$u_* = \sqrt{\tau_0/\rho} = \sqrt{\rho g h S_f/\rho} = \sqrt{g h S_f} \tag{4}$$

where τ_0 is the boundary shear stress, ρ is the density of water, g is the gravitational acceleration, h is the flow depth, and S_f is the local friction slope (Dey 2014). Consequently, instead of a constant value of u_*, one might expect that the friction velocity is proportional to the square root of the local depth. Therefore, assuming that the friction slope and gravity are constants along the section, the shear velocity can be written as $u_* = c_2\sqrt{h}$, where c_2 is a constant. As a result, Eq. (2) can be written as

$$u(y,z) = \int_{boundary} c\sqrt{h} \sin\theta r^{1/m} d\mathbf{s} \tag{5}$$

where h is the local water depth where the boundary element $d\mathbf{s}$ is, and c is a constant related to the boundary geometry, relative roughness, and the friction slope. Due to the relative relation of Eq. (3), the exact value of c is unnecessary, but the variation of c along the section is significant.

Dip Phenomenon

One of the benefits of the Maghrebi (2006) method is its ability to use any velocity distribution. There exist various velocity distributions that deal with the velocity dip phenomenon. The PWL derived by Guo (1998) is used herein as a velocity function because of its simplicity and algebraic form. The PWL has the following form:

$$\frac{u}{u_*} = C_0\xi^{\alpha} + \Omega_0 \sin^2\frac{\pi\xi}{2} + \alpha C_0(1-\xi) \tag{6}$$

where C_0, Ω_0, and α are constants, $\xi = z/\delta$, and δ is the boundary layer thickness defined as the distance from the channel bed to the maximum velocity location. The first term represents the power law, the second is the Coles wake correction function, and the third is the boundary correction function. The effect of the wake term is weak, and the boundary correction is more significant when considering the dip phenomenon. Therefore, the wake term could be neglected. Considering Eq. (6) as a velocity function, Eq. (2) can be written as

$$u(y,z) = \int_{boundary} cu_*\xi^{1/m} \sin\theta d\mathbf{s} + \int_{boundary} \alpha c u_*(1-\xi)\sin\theta d\mathbf{s} \tag{7}$$

where $\xi = r/\delta$, $\delta = \beta R_w$, and R_w is the distance from the boundary element $d\mathbf{s}$ through the target flow element to the opposite boundary (see Fig. 1).

For this model, the coefficient c is assumed to be like the previous model (i.e., unity value for uniform roughness boundary, inversely proportional with roughness changing) and 0.3 for the water surface boundary. The analysis of α and β effects is introduced in the "Results" section.

Velocity and Discharge

Calculating the normalized local velocity $C(y,z)$ at different points allows drawing the isovel contours and thus calculating the discharge. Obtaining the flow requires measuring at least one local point velocity besides calculating the corresponding normalized local velocity. The discharge can be obtained as follows:

$$Q = A\frac{v(y,z)}{C(y,z)} \tag{8}$$

where $v(y,z)$ is the measured local velocity. The resulting discharge errors are calculated as follows:

$$Error(\%) = \frac{Q_c - Q_o}{Q_o} \times 100 \tag{9}$$

where Q_c and Q_o are the estimated and observed discharges, respectively.

The results of this method show that its accuracy is associated with the position of the observed point at the cross-section, and substantial errors might happen in some cases. Therefore, more than one measurement point is used to estimate the flow to ensure

the best accuracy with minimum effort. A combination approach is used to demonstrate the performance of the modifications and the impact of an increasing number of measurements. The following approach is applied to the field data:

1. All possible combination sets of Comb_n are constructed. A combination of $2, 3,$ and $\ldots 10$ velocity measurement points can lead to $\text{Comb}_2, \text{Comb}_3, \ldots,$ and Comb_{10}, respectively.
2. For each set of Comb_n sets, the discharge is estimated for each point using Eq. (8).
3. Then, the estimated discharge representing the set is obtained by simply using the average value. This step is carried out for all Comb_n sets.
4. Using the computed discharges from the previous step, the mean absolute percent error (MAPE) value is calculated from the following equation:

$$MAPE = \frac{100}{N}\sum_{i=1}^{N}\left|\frac{Q_o - (Q_c)_i}{Q_o}\right| \tag{10}$$

where N is the number of sets of a selected combination, and Q_c is the average calculated discharge of each set.

Case Studies

Published velocity data from Nihei and Kimizu (2008), Moramarco et al. (2004), Singh (2014), Cheng et al. (2004), Culbertson et al. (1972), and HBYRCC (2019) are used herein. Cross-sections of the Yellow River in China, the Edo River in Japan, the Tiber and the Chiascio Rivers in Italy, and the San Joaquin River the Rio Grande Channel in the United States were used to evaluate the performance of the proposed method. The velocity data of these sections were collected using current meters or an acoustic Doppler current profiler (ADCP). The flow and site characteristics for the six rivers are shown in Table 1. Fig. 2 shows the topographical surveys of the selected cross-sections and the observed points' position.

Results

Determination of the Model's Parameters

To obtain the water surface coefficient cw, the PL-based model is applied to different rectangular channels available in the literature with different width-depth ratios (aspect ratios). Table 2 shows the hydraulic characteristics of the laboratory sections used to calibrate the cw coefficient. All the laboratory sections used in this study are hydraulically smooth wall open channels. From Fig. 3, it is evident that the model overestimates the velocity near the water surface and underestimates it near the bed for larger aspect ratios. Since the water surface boundary has no roughness, the magnitude of cw must be assessed as a ratio of the rest wall resistances. Using a trial-and-error procedure, different values of cw are examined, from 0.1 of other wall resistances to 0.7, and the MAPE value is calculated for each case. Fig. 4 shows MAPE values for different sections and various values of cw. This figure illustrates that cw in the range between 0.3 and 0.4 produces minimum MAPE values in most cases, particularly when $Ar > 1.67$. Therefore, $cw = 0.3$ is selected as an appropriate value to be used for the modified model.

Similarly, a trial-and-error procedure obtains the constants α and β in the PWL-based model. The parameter β specifies the thickness of the layer above which the boundary correction begins to reduce the velocity, whereas the parameter α controls the intensity of the boundary correction. The ranges of the constants α and β are assumed to be from 0 to $2/m$ and 0.5 to 1, respectively, where

Table 1. Summary of hydraulic and geometric conditions for the study sites

Site name	Water course	Type	Date	B (m)	D (m)	P (m)	R (m)	F	n	S_0 ($\times 10^{-4}$)	Q (m^3/s)	V (m/s)	Source
Huayuankou	Yellow	Asymmetric	March 21, 2019	310	6.40	312	2.69	0.28	0.031	5.09	1,370	1.49	HBYRCC (2019)
Noda	Edo	Simple	October 13, 2005	62	2.93	63	2.20	0.12	0.035	—	78.6	0.57	Nihei and Kimizu (2008)
Ponte Nuovo	Tiber	Simple	June 3, 1997	54	6.31	58	4.75	0.25	0.061	14	541.6	1.74	Singh (2014)
Rosciano	Chiascio	Simple	May 28, 1984	37	3.20	40	2.58	0.34	0.047	19.8	156.2	1.78	Moramarco et al. (2004)
Section 250	Rio Grande	Simple	June 11, 1969	23	1.95	25	1.37	0.30	0.026	5.7	39.3	1.13	Culbertson et al. (1972)
Vernalis	San Joaquin	Asymmetric	May 17, 2002	69	2.4	69	1.62	0.40	—	—	112.3	1.61	Cheng et al. (2004)

Note: B is the channel width, D is the maximum depth, P is the wetted perimeter, R is the hydraulic radius, F is the Froude number, n is Manning's roughness, S_0 is the channel bed slope, and V is the mean channel velocity.

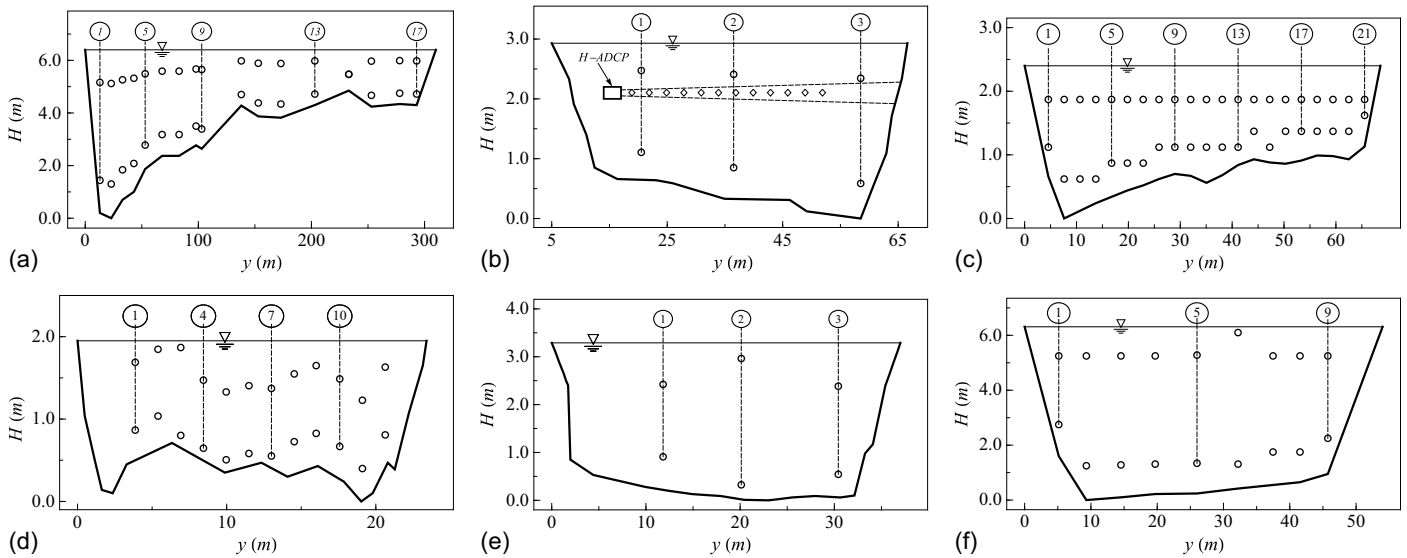

Fig. 2. Topographical surveys of the (a) Yellow River; (b) Edo River; (c) San Joaquin River; (d) Rio Grande Channel; (e) Chiascio River; and (f) Tiber River.

Table 2. Summary of hydraulic and geometric conditions for rectangular sections

Section	B (cm)	h (cm)	Ar	Q (l/s)	S_0	F	Source
S1	40	40	1	13.7	7.6×10^{-6}	0.04	Maghrebi (2006)
S2	40	32	1.25	14.7	1.5×10^{-5}	0.06	Maghrebi (2006)
S3	40	24	1.67	15.6	3.6×10^{-5}	0.11	Maghrebi (2006)
S4	26.7	6.5	4.1	11.5	2.06×10^{-3}	0.83	Lyn (1988)
S5	26.7	5.7	4.7	13.2	4.01×10^{-3}	1.16	Lyn (1988)
S6	60	10	6	29	6.7×10^{-4}	0.49	Nezu and Rodi (1986)
S7	91	13	7	73.8	7.41×10^{-4}	0.05	Muste and Patel (1997)
S8	200	15.2	13	53	—	0.14	Johnson (2015)

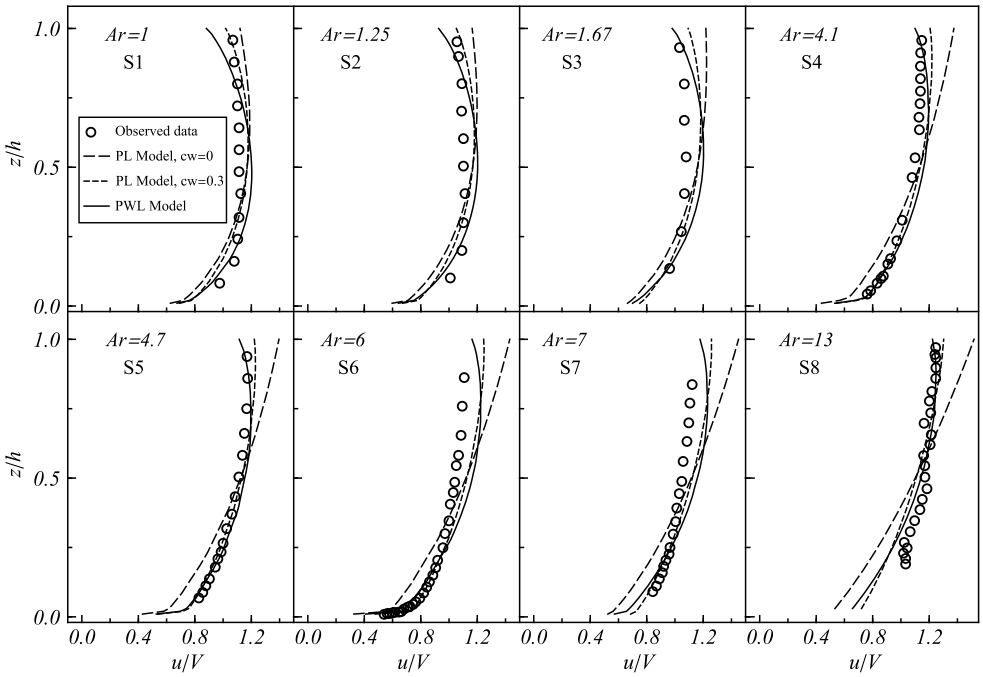

Fig. 3. Centerline computed velocity profile with observed data from Johnson (2015), Lyn (1988), Maghrebi (2006), Muste and Patel (1997), and Nezu and Rodi (1986); cw is the water surface coefficient.

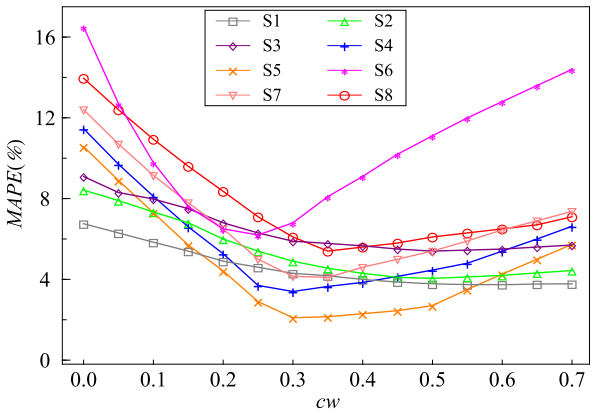

Fig. 4. MAPE values for different sections and different values of water surface coefficient cw.

$m = 7$. MAPE values of all steps and all sections are shown in Fig. 5. The figure illustrates that the lines related to $\beta = 0.5$ and $\beta = 0.6$ present the lowest MAPE values, particularly when $Ar > 1.25$. For $\beta > 0.6$, the variation of MAPE values with α is slight. Whereas for β equals 0.5 or 0.6, $\alpha = 1.5/m$ produces better results. Therefore, $\alpha = 1.5/m$ and $\beta = 0.6$ are selected as appropriate values that yield minimum MAPE values in most cases.

The centerline estimated velocity profiles of the laboratory sections compared to the observed ones are shown in Fig. 3. Improving the estimation of the upper portion of the vertical velocity profile is a potential benefit of the PWL-based model. A comparison between the performance of the PL and PWL-based models in terms of MAPE for points higher than $0.2h$ is shown in Fig. 6. The figure illustrates that the PWL-based model has reduced the velocity errors in the upper portion of flow.

Velocity Profiles

Based on the proposed models, the isovel contours and velocity profiles can be drawn in any vertical within the cross-section. Fig. 7 shows the estimated and observed velocity profiles in five rivers. The Yellow River velocity profiles are not included in the figure because only two measured points are available in each vertical. MAPE values of each profile are shown next to each vertical in the figure. For all velocity profiles, the main PL-based model without modifications overestimates the velocity near the water surface and underestimates it close to the bed. Considering the water surface coefficient has improved the results. Due to the observed dip phenomenon in the Edo, Chiascio, and Tiber Rivers, the PWL-based model profiles best fit the observed data. Even in the absence of the dip velocity in the San Joaquin River, the performance of PWL is still acceptable.

Discharge Estimation

Calculations were performed to estimate the discharge using every observed point. The MAPE values of the Yellow River are 22% for the basic PL model without modifications, 18% when $cw = 0.3$, 11% when considering water surface effect and variable shear velocity, and 11% for the PWL-based model. The results demonstrate that both the water surface coefficient and shear velocity variation with the square root of h increase the accuracy.

The results show relatively high errors when estimating discharge with a single point in the Tiber River. The MAPE values are 34% for the basic PL model without modifications, 23% when $cw = 0.3$, 23% when considering water surface effect and variable shear velocity, and 22% for the PWL-based model. For all other case studies, the resulting MAPE values for the basic PL model, without modifications, are 14%–25%, which are reduced to 7%–12% when applying the water surface coefficient.

Whereas the water surface coefficient improves the outcomes significantly in all studied cases, there is no effect of the shear velocity variation with the square root of h. The shear velocity variation with the square root of h has improved the results only in the Yellow River cross-section. The performance of the PL-based model is the same as that of the PWL-based model, with a relative superiority of the PWL-based model.

Combination Approach

The combination approach described in the previous section is applied to the field data to explore the performance of the modifications and the impact of increasing the number of measurements. For clarification, the combination methodology is implemented for two-point combinations ($Comb_2$) in the Yellow River. There exist 34 measured points in the Yellow River cross-section (17 points at $0.2h$ and 17 points at $0.8h$). In step 1, each fixed measuring point at

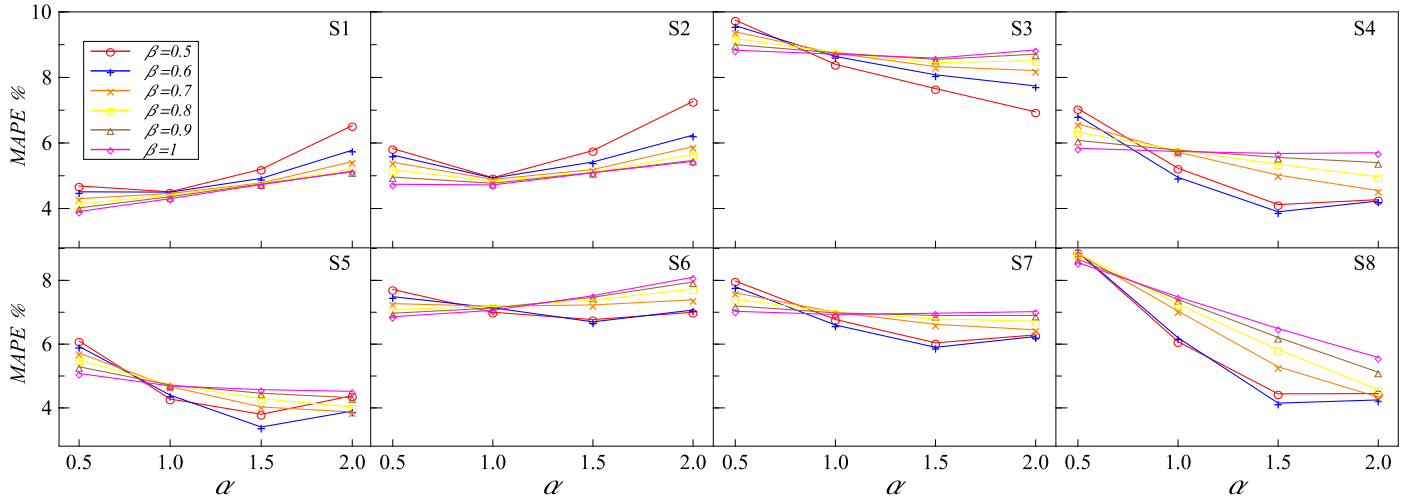

Fig. 5. MAPE values for different sections and different values of PWL-based model parameters, α and β.

J. Hydraul. Eng., 2023, 149(11): 06023008

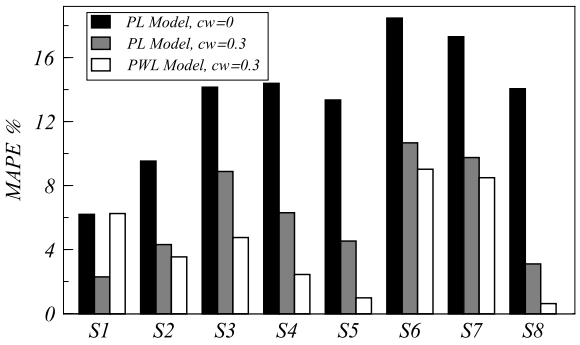

Fig. 6. MAPE values computed based on points higher than $0.2h$ in the laboratory sections.

$h = 0.8h$ is connected to 17 variable points, each one at $0.2h$. Therefore, the total number of combinations will equal $17 \times 17 = 289$ combination sets. Steps 2 to 4 are performed to compute the MAPE for Comb_2. The same procedure is repeated for three-point combinations (Comb_3), four-point combinations (Comb_4)..., and 10-point combinations (Comb_{10}). Comb_3 sets are constructed using two $0.8h$ points with one $0.2H$ point resulting in 2,312 cases. Comb_4 sets are built using two $0.2h$ points with two $0.8H$ points (36,992 sets), etc. Fig. 8(a) shows the MAPE values for the different combinations. The results indicate that increasing the number of used measured points improves accuracy efficiently. A combination of five arbitrary points lowers the error to less than 8% for the basic PL model without modifications, 6% when $cw = 0.3$, 4% when considering water surface effect and variable shear velocity, and 5% for the PWL-based model.

The combination approach was repeated for all cross-sections. For this purpose, two points at $0.2h$ and $0.8h$ for each vertical line were chosen to construct the combination sets. If no measured velocity data at $0.2h$ and $0.8h$ were available, the closest observed points to those locations were selected. As seen from Fig. 8, the three-point combinations reduce the discharge error to less than 5% regardless of fixed points in the Edo and Chiascio Rivers. The five-, six-, and seven-point combinations reduce the discharge error to less than 5% in the San Joaquin, Rio Grande, and Tiber Rivers.

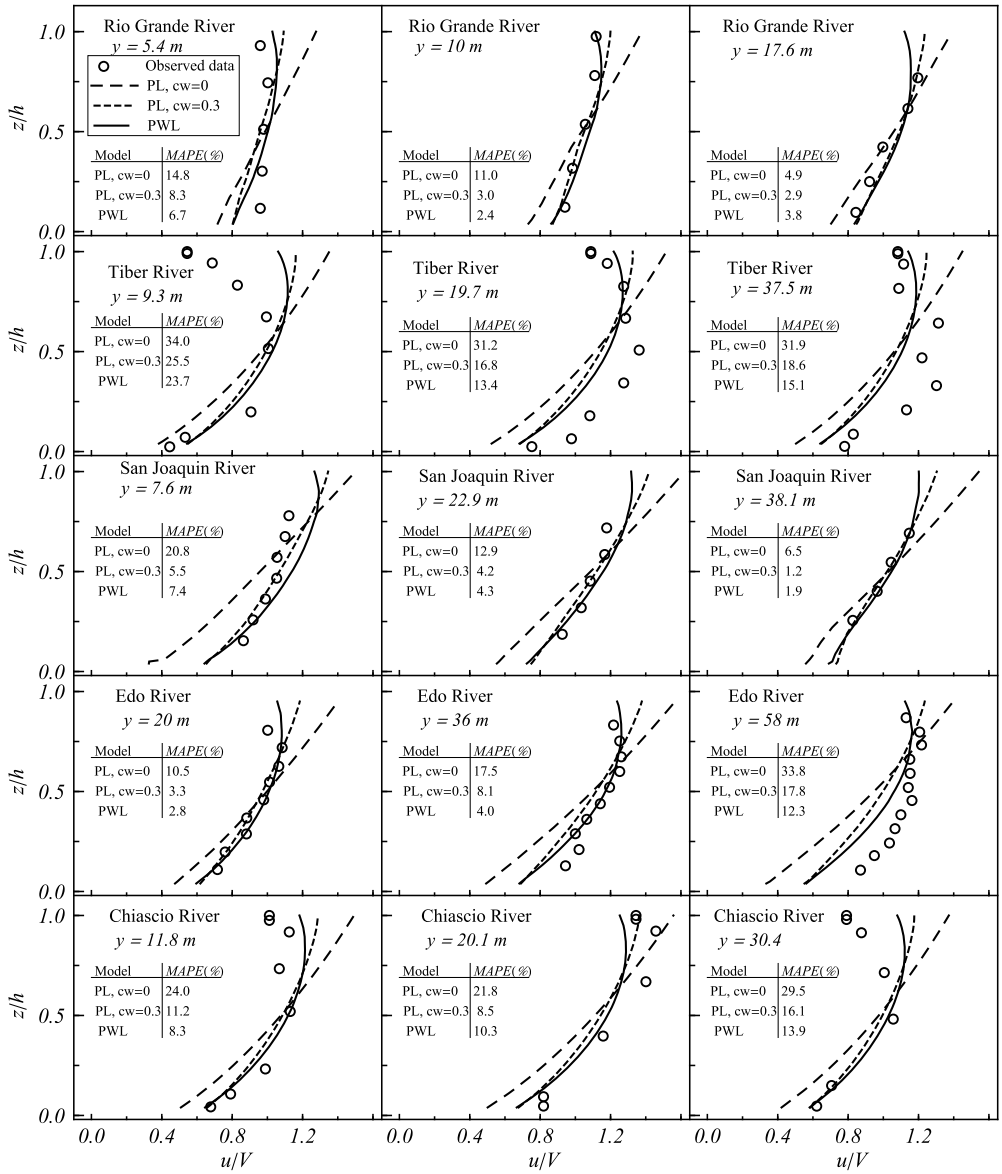

Fig. 7. Computed velocity profiles compared with observed profiles for selected river cross-sections.

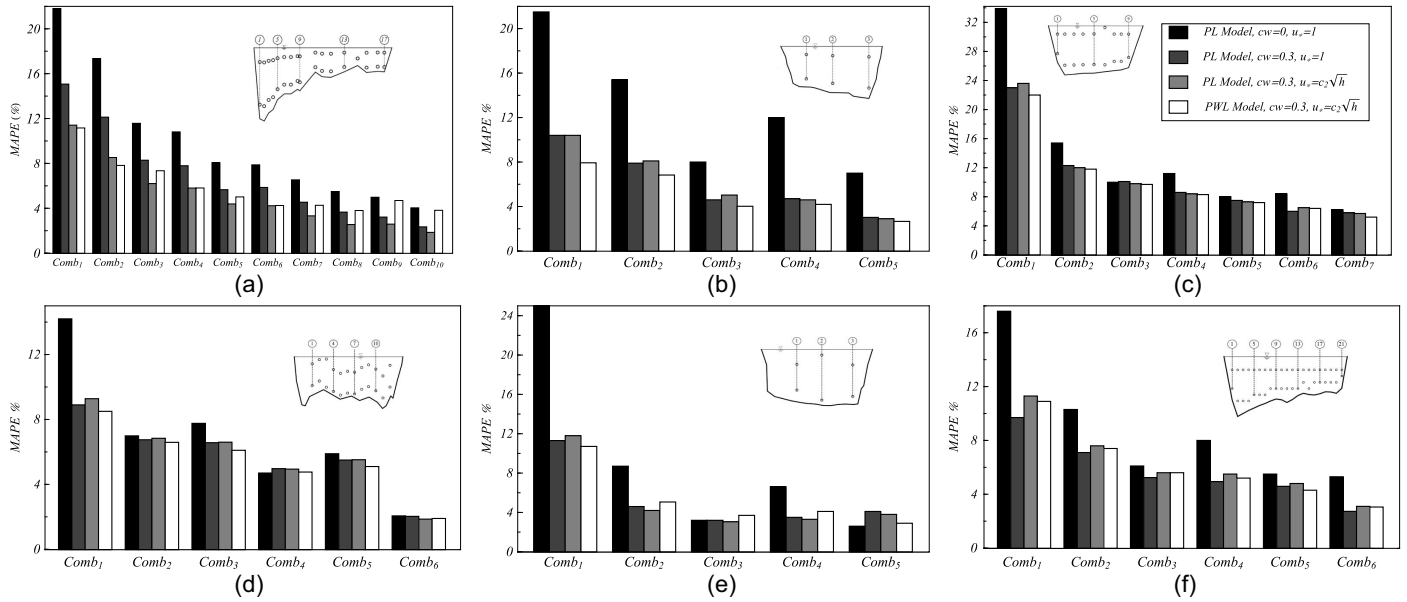

Fig. 8. MAPE values of the estimated discharges for various combinations for the studied river cross-sections. The Comb$_n$ refers to a combination of n points: (a) Yellow River; (b) Edo River; (c) Tiber River; (d) Rio Grande Channel; (e) Chiascio River; and (f) San Joaquin River.

In addition, it can be seen from Fig. 8 that there is no effect of the shear velocity variation with the square root of h on results. The water surface coefficient is the most critical for improving outcomes.

Single-Point Measurement

It is interesting to know how discharge errors are distributed along the cross-section if only one velocity point is used to estimate discharge. For this purpose, the error distribution was stated as a function of isovel contours magnitudes C. The higher values of C correspond to the upper parts of the cross-section near the water surface, whereas parts close to the boundary get small C values. Figs. 9(a–f) shows the computed errors corresponding to each measured velocity point plotted against C for all studied cross-sections. As seen from Fig. 9, the magnitudes of errors generally decrease for larger values of C and increase for lower ones. The most significant errors correspond to $C < 1$ for most cross-sections, whereas the minimum errors correspond to $C > 1$. $C \approx 1.15$ corresponds to a discharge error of less than 2% for the PWL model in the six studied cross-sections.

To identify the potential locations that produce minor errors, the distribution of points satisfying the conditions $C > 1$ and $z/h > 0.5$ along the cross-section was represented in Fig. 10. Black and gray symbols are associated with discharge errors less than and larger than 10%, respectively. The figure shows that the area bounded by $0.5 < z/h < 0.8$ and $0.2 < y/B < 0.8$ is the region that is likely to produce low errors. MAPE values for all points that

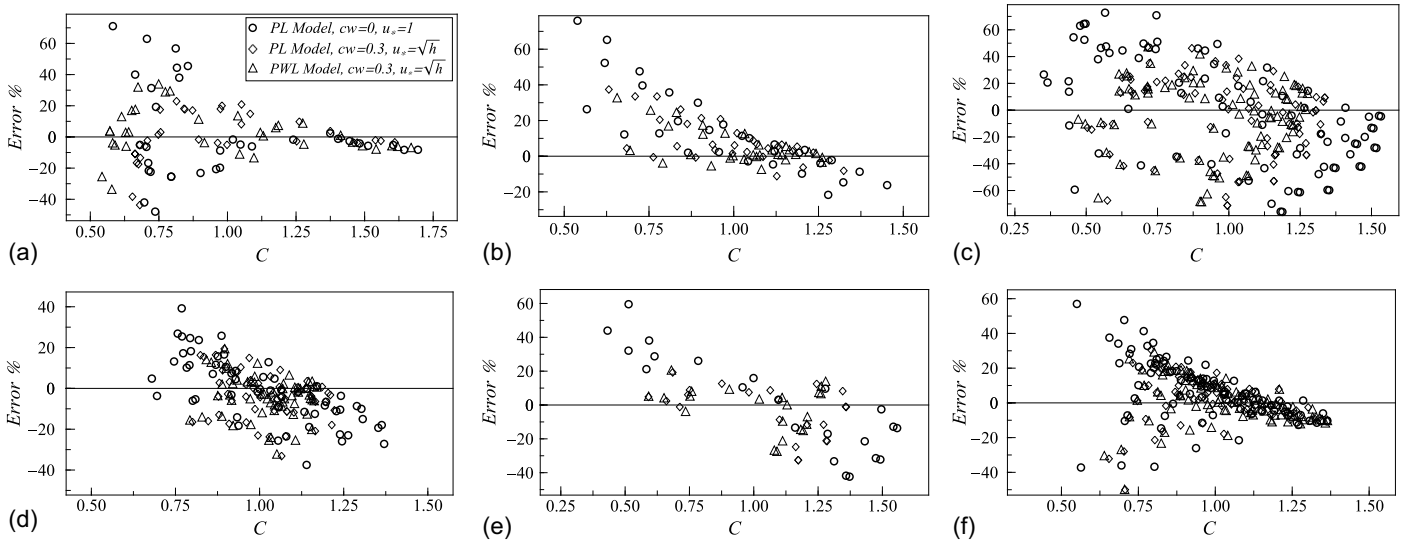

Fig. 9. Variation of discharge errors as a function of isovel lines C for the cross-sections of the (a) Yellow River; (b) Edo River; (c) Tiber River; (d) Rio Grande Channel; (e) Chiascio River; and (f) San Joaquin River.

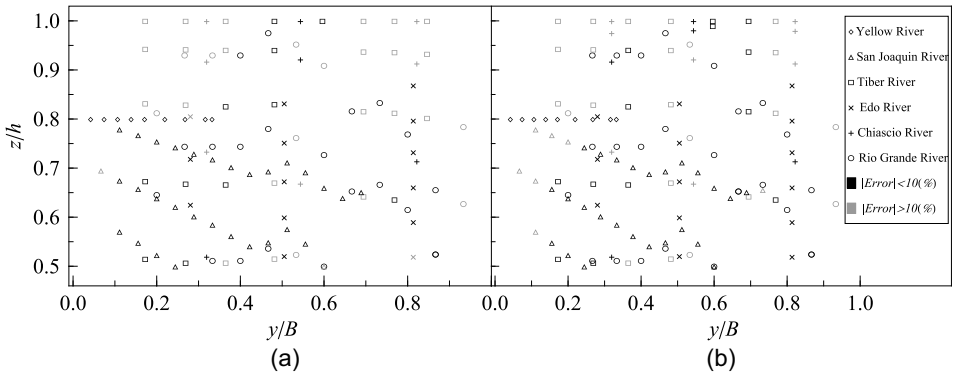

Fig. 10. Distribution of points satisfying the conditions $C > 1$ and $z/h > 0.5$ along each cross-section of the studied rivers: (a) PL-based model; and (b) PWL-based model.

satisfy all conditions in the six selected rivers are 7.9% for the modified PL-based model and 7.3% for the PWL-based model.

Conclusion

This work presented modifications to the PL-based model and the SPM method for calculating channel discharge. After analyzing the effects of the free water surface and shear velocity, modifications to the model were proposed. In addition, the PWL velocity distribution was presented as a velocity function to deal with the velocity dip phenomenon. A combination of more than one measurement point was used to estimate the discharge to minimize errors, costs, and time. MAPE values were used to measure the accuracy. The findings are in brief:

- The PL model Maghrebi (2006), without any modifications, overestimates the velocity near the water surface and underestimates it near the bed for wider channels. Considering water surface coefficient $cw = 0.3$ has improved the results significantly.
- Whereas the water surface coefficient improves the outcomes significantly, there is no effect of the shear velocity variation with the square root of h on results. The shear velocity variation with the square root of h has improved the results only in the Yellow River cross-section.
- The modified PL- and PWL-based models can estimate discharge with reasonable accuracy using five measured velocimetry points in most tested cross-sections. The points were distributed randomly at $0.2h$ and $0.8h$. In most case studies, the five-point combinations reduce the MAPE values to less than 5%.
- The PWL-based model performs better than the PL-based model when the dip velocity occurs. MAPE values for one point for the Edo River are 10% and 7% for the PL and the PWL-based models, respectively.
- The estimated discharge errors based on only one velocity point decrease for larger values of isovel contour C and increase for lower values. In the case of $C > 1$, it is found that the area bounded by $0.5 < z/h < 0.8$ and $0.2 < y/B < 0.8$ is the region that is likely to produce low errors.

The results demonstrated that the method applies to a wide range of relatively straight rivers. However, significant errors might be produced near bank sides due to the variation of the roughness along the cross-section. Therefore, further studies in sections with heterogeneous roughness and meandering channels are required.

Data Availability Statement

All data, models, or code that support the findings of this study are available from the corresponding author upon reasonable request (Ali and Maghrebi 2023). Some of the data and code are available online for the public (http://www.hydroshare.org/resource/d8df4d9fdd874cb6a66fa2495e61ab09).

Notation

The following symbols are used in this paper:

A = flow area;
Ar = width to depth ratio;
B = channel width;
C = normalized local velocity;
c = boundary coefficient;
cw = water surface coefficient;
D = maximum depth;
dA = area of each computational mesh;
$d\mathbf{s}$ = boundary element;
F = Froude number;
$f(r)$ = velocity function;
g = gravitational acceleration;
H = channel stage;
h = water depth;
m = exponent of the power law;
n = Manning's roughness;
P = wetted perimeter;
Q = discharge;
Q_c = computed discharge;
Q_o = observed discharge;
R = hydraulic radius;
R_w = distance from the boundary element $d\mathbf{s}$ to the opposite boundary;
$\mathbf{r}$ = positional vector;
S_0 = channel bed slope;
S_f = friction slope;
U = computational mean velocity;
u = computational local velocity;
u_* = shear velocity;
V = mean channel velocity;
v = local velocity;

y = horizontal coordinate;
z = vertical coordinate;
α, β = power-wake-law constants;
δ = boundary layer thickness;
Ω_0 = constant;
ρ = density of water;
ξ = ratio of the distance from the bed, z to boundary layer thickness;
τ_0 = boundary shear stress; and
θ = angle between the positional vector r and the boundary elemental vector $d\mathbf{s}$.

References

Ali, G., and M. F. Maghrebi. 2023. "Modifications to the single point velocity measurement method for estimating river discharge in low-resource environments." HydroShare. Accessed August 19, 2023. http://www.hydroshare.org/resource/d8df4d9fdd874cb6a66fa2495e61ab09.

Cheng, R. T., J. W. Gartner, R. R. Mason Jr., J. E. Costa, W. J. Plant, K. R. Spicer, F. P. Haeni, N. B. Melcher, W. C. Keller, and K. Hayes. 2004. *Evaluating a radar-based, noncontact streamflow measurement system in the San Joaquin River at Vernalis, California*. Rep. No. 2004-1015. Washington, DC: USGS.

Culbertson, J. K., C. H. Scott, and J. P. Bennett. 1972. *Summary of alluvial-channel data from Rio Grande conveyance channel, New Mexico, 1965–69*. Washington, DC: US Government Printing Office.

Dey, S. 2014. "Turbulence in open-channel flows." In *Fluvial hydrodynamics*, 95–187. New York: Springer.

Fulton, J. W., I. E. Anderson, C.-L. Chiu, W. Sommer, J. D. Adams, T. Moramarco, D. M. Bjerklie, J. M. Fulford, J. L. Sloan, and H. R. Best. 2020. "QCam: SUAS-based Doppler radar for measuring river discharge." *Remote Sens.* 12 (20): 3317. https://doi.org/10.3390/rs12203317.

Guo, J. 1998. "Turbulent velocity profiles in clear water and sediment-laden flows." Ph.D. thesis, Dept. of Civil Engineering, Colorado State Univ.

HBYRCC (Hydrology Bureau Yellow River Conservancy Commission). 2019. "Yellow river hydrographic survey and mapping bureau." Accessed August 19, 2023. https://www.hwswj.gov.cn.

Johnson, E. 2015. "The remote monitoring of surface velocity, bathymetry and discharge in rivers and open channel flows." Ph.D. thesis, Faculty of the Graduate School, Cornell Univ.

Lyn, D. 1988. "A similarity approach to turbulent sediment-laden flows in open channels." *J. Fluid Mech.* 193 (Aug): 1–26. https://doi.org/10.1017/S0022112088002034.

Maghrebi, M. F. 2006. "Application of the single point measurement in discharge estimation." *Adv. Water Resour.* 29 (10): 1504–1514. https://doi.org/10.1016/j.advwatres.2005.11.007.

Maghrebi, M. F., and J. E. Ball. 2006. "New method for estimation of discharge." *J. Hydraul. Eng.* 132 (10): 1044–1051. https://doi.org/10.1061/(ASCE)0733-9429(2006)132:10(1044).

Moramarco, T., C. Saltalippi, and V. P. Singh. 2004. "Estimation of mean velocity in natural channels based on Chiu's velocity distribution equation." *J. Hydrol. Eng.* 9 (1): 42–50. https://doi.org/10.1061/(ASCE)1084-0699(2004)9:1(42).

Muste, M., and V. Patel. 1997. "Velocity profiles for particles and liquid in open-channel flow with suspended sediment." *J. Hydraul. Eng.* 123 (9): 742–751. https://doi.org/10.1061/(ASCE)0733-9429(1997)123:9(742).

Nezu, I., and W. Rodi. 1986. "Open-channel flow measurements with a laser Doppler anemometer." *J. Hydraul. Eng.* 112 (5): 335–355. https://doi.org/10.1061/(ASCE)0733-9429(1986)112:5(335).

Nihei, Y., and A. Kimizu. 2008. "A new monitoring system for river discharge with horizontal acoustic Doppler current profiler measurements and river flow simulation." *Water Resour. Res.* 44 (4): W00D20. https://doi.org/10.1029/2008WR006970.

Singh, V. P. 2014. *Entropy theory in hydraulic engineering: An introduction*. Reston, VA: ASCE.

Welber, M., J. Le Coz, J. B. Laronne, G. Zolezzi, D. Zamler, G. Dramais, A. Hauet, and M. Salvaro. 2016. "Field assessment of noncontact stream gauging using portable surface velocity radars (SVR)." *Water Resour. Res.* 52 (2): 1108–1126. https://doi.org/10.1002/2015WR017906.